Parametric Representations of Neutron-Star Equations of State With Phase Transitions

Lee Lindblom
Department of Physics, University of California at San Diego
(Dated: June 19, 2024)

This paper explores the use of low-dimensional parametric representations of neutron-star equations of state that include discontinuities caused by phase transitions. The accuracies of optimal piecewise-analytic and spectral representations are evaluated for equations of state having first- or second-order phase transitions with a wide range of discontinuity sizes. These results suggest that the piecewise-analytic representations of these non-smooth equations of state are convergent, while the spectral representations are not. Nevertheless, the lower-order ($2 \leq N_{\rm parms} \leq 7$) spectral representations are found to be more accurate than the piecewise-analytic representations with the same number of parameters.

I. INTRODUCTION

The equation of state of the material in the cores of neutron stars is not well known at this time. The density of this material far exceeds the limits of current laboratory experiments, and there is at present no universally accepted theoretical model of this material. Astrophysical observations of neutron stars can in principle be used to determine the neutron-star equation of state [1]. However, the quality and quantity of those observations are presently quite limited.

Parametric representations of the neutron-star equation of state have been introduced as a way to analyze the results of the relevant astrophysical observations. The parameters in these equations of state are adjusted to provide best-fit models of the observational data, thus producing approximate representations of the physical equation of state. Since the quality and quantity of the relevant astrophysical observations are still quite limited, parametric representations that provide good accuracy using only a small number of parameters are needed.

Two types of parametric representations of the equation of state have been introduced for this purpose. Piecewise-analytic representations, first introduced in Ref. [2], divide the range of densities into discrete ranges with parameter-dependent analytic expressions representing the equation of state within each range. Another type of parametric representation, first introduced in Ref. [3], is constructed from a generating function expressed as a linear combination of fixed basis functions, e.g. polynomial or trigonometric functions. The parameters in these "spectral" representations are the coefficients that multiply the basis functions in the sum that determines the generating function for the equation of state.

The accuracies of both the piecewise-analytic and the spectral representations have been evaluated using a diverse collection of theoretical neutron-star equation of state models [2–5]. Those tests showed that both types of representation are convergent in the sense that their accuracies increased as the number of parameters in the representation increased. Those tests also showed that reasonably good accuracies (at the few percent level) could be achieved with representations having a fairly small number of parameters. Consequently both the piecewise-analytic and the spectral representations have been widely used to analyze the presently available observational data, with Refs. [2] and [3] having received hundreds of citations in the literature.

Previous tests of the accuracy of these parametric representations used a collection of mostly discontinuity-free theoretical equation of state models. The physical neutron-star equation of state may (or may not) include discontinuities caused by phase transitions. The purpose of this paper is to systematically evaluate the accuracy of the piecewise-analytic and the spectral representations when used to represent non-smooth neutron-star equations of state with phase transitions. A sequence of exemplar equations of state are constructed in Appendix A for this study with phase transitions having a range of sizes. Those exemplar equations of state are then used to test the accuracy of both the piecewise-analytic and the spectral representations.

The methods used in this study to construct optimal parametric equation of state fits are described in Sec. II. These methods are then used to construct optimal fits to each exemplar equation of state using both the piecewise-analytic and the spectral representations. The accuracies of the resulting optimal fits are evaluated using the L_2 norm of the difference between the exemplar equation of state and its parametric representation. These results illustrate how the accuracies of the parametric representations depend on the type of representation (piecewise analytic or spectral), the size and type (first- or second-order) of the phase-transition discontinuities, and the orders of the parametric representations.

Section III discusses the implications of the results found here. If and when more accuracy is needed to model future improvements in the quality and quantity of observational data, a split domain method for constructing more accurate representations of non-smooth equations of state with phase transitions is proposed.

II. OPTIMAL PARAMETRIC FITS

This section describes the method used in this study to test the accuracy of optimal piecewise-analytic and spectral representations of neutron-star equations of state with phase transitions. The exemplar equations of state with phase transitions used to perform these tests were constructed from the relatively smooth GM1L equation of state, which is based on a mean-field representation of the interactions between nucleons [6]. Discontinuities representing first- or second-order phase transitions were inserted into a tabulated representation of GM1L at a point several times nuclear density where the energy density has the value $\epsilon_T = 8 \times 10^{14}$ g/cm^3. These discontinuities were inserted with a range of sizes specified by a parameter k, which determines the size of the discontinuity as a fraction of the maximum physically relevant discontinuity (see Appendix A). The family of exemplar equations of state used in this study range from the original smooth GM1L equation of state with $k = 0$ to equations of state with the maximum discontinuity of each type with $k = 100$. Details of the construction of these exemplar equations of state are given in Appendix A. Figures 1 and 2 illustrate members of these exemplar equation of state families, with first- and second-order phase transitions respectively, in the neighborhood of the phase transition point.

The particular parametric equation of state representations used in this study [3, 5] are described in Appendix B. These parametric representations are causal in the sense that the sound speeds are less than the speed of light for every choice of the parameters. The representations used in this study express the energy density $\epsilon(h, \upsilon_a)$ and the pressure $p(h, \upsilon_a)$ as functions of the enthalpy h of the fluid and a set of parameters υ_a for $1 \le a \le N_{\rm parms}$. This type of representation is most useful when using the enthalpy-based form of the relativistic stellar structure equations [1]. This form of the equations allows numerical determinations of the masses and radii more accurately and more efficiently than the standard pressure-based Oppenheimer-Volkoff [7] form. The families of exemplar equations of state with phase transitions described in Appendix A were produced as enthalpy-based tables, $\{\epsilon_i, p_i, h_i\}$ for $0 \le i \le N_{\rm table}$, to facilitate comparisons with the enthalpy-based parametric representations.

The next step is to find the values of the parameters υ_a in the equation of state, $\epsilon(h, \upsilon_a)$, that best approximates one of the exemplar equations of state. The optimal parameter values υ_a are found in this study by minimizing the function $\chi(\upsilon_a)$ that measures the average difference between the tabulated values of the exemplar equation of state, $\epsilon_i(h_i)$, and the corresponding values from the parametric equation of state, $\epsilon(h_i, \upsilon_a)$:

$$\chi^2(\upsilon_a) = \frac{1}{N_{\rm table}} \sum_{i=0}^{N_{\rm table}} \left[\log\left(\frac{\epsilon(h_i, \upsilon_a)}{\epsilon_i(h_i)} \right) \right]^2 . \qquad (1)$$

The error function $\chi^2(\upsilon_a)$ is non-negative, and therefore

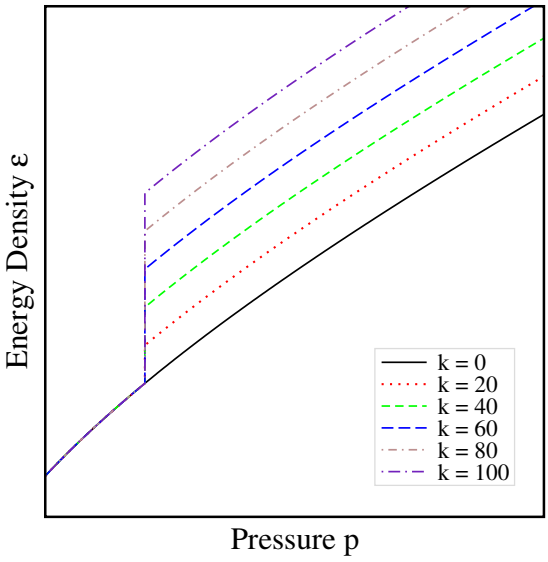

FIG. 1: Several exemplar equations of state with first-order phase transitions are illustrated in a neighborhood of the phase transition point. The curves shown here include the original GM1L equation of state, $k = 0$, and several equations of state with larger density offsets, $0 < k \le 100$. The $k = 100$ curve has the maximum density offset allowed in stable (and therefore observable) neutron-stars.

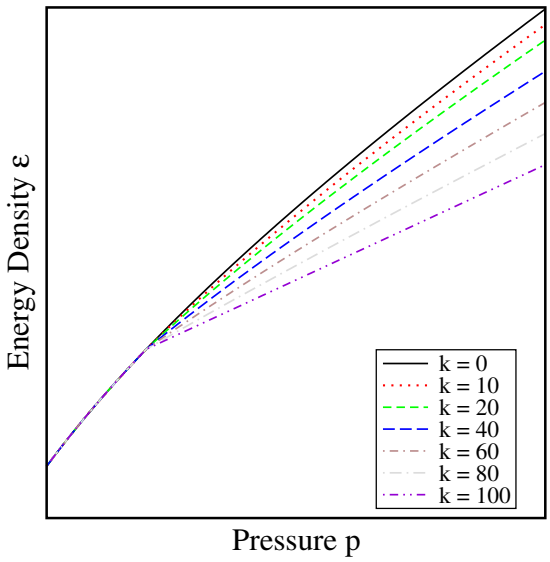

FIG. 2: Several exemplar equations of state with second-order phase transitions are illustrated in a neighborhood of the phase transition point. The curves shown here include several equations of state with density derivative offsets in the range $0 \le k \le 100$. The $k = 0$ curve represents the original GM1L equation of state, and the $k = 100$ curve has the largest physically possible fluid-velocity discontinuity, with the fluid velocity equal to the speed of light on the high density portion of this curve.

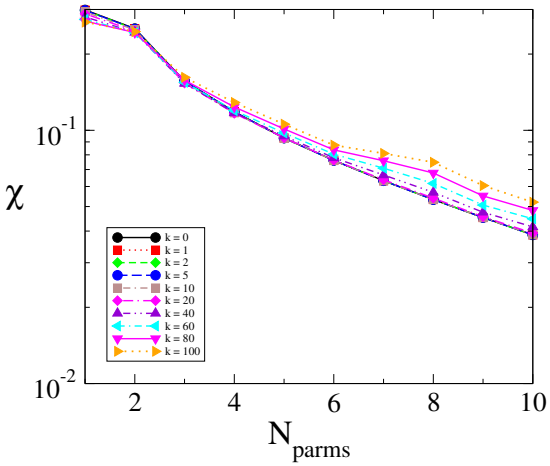

FIG. 3: Average errors $\chi(N_{\rm parms})$ for the piecewise-analytic fits as a function of $N_{\rm parms}$ for a family of equations of state with first-order phase transitions of various sizes, $0 \leq k \leq 100$.

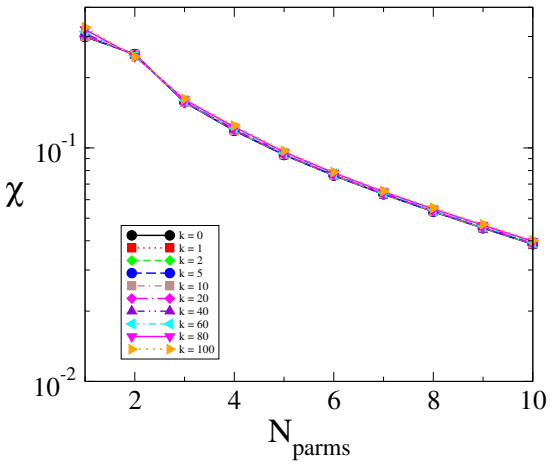

FIG. 4: Average errors $\chi(N_{\rm parms})$ for the piecewise-analytic fits as a function of $N_{\rm parms}$ for a family of equations of state with second-order phase transitions of various sizes, $0 \leq k \leq 100$.

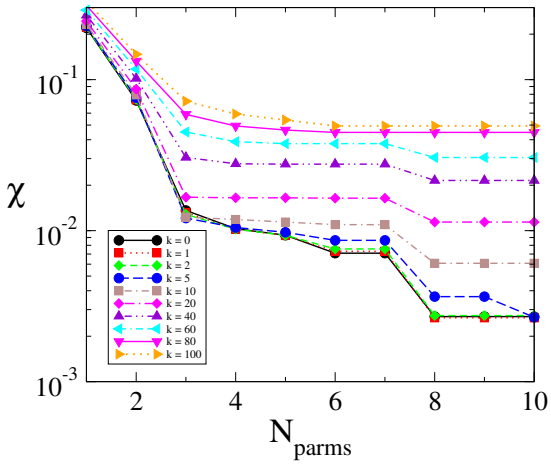

FIG. 5: Average errors χ for the optimal spectral fits as a function of $N_{\rm parms}$ for a sequence of equations of state with first-order phase transitions of various sizes, $0 \leq k \leq 100$.

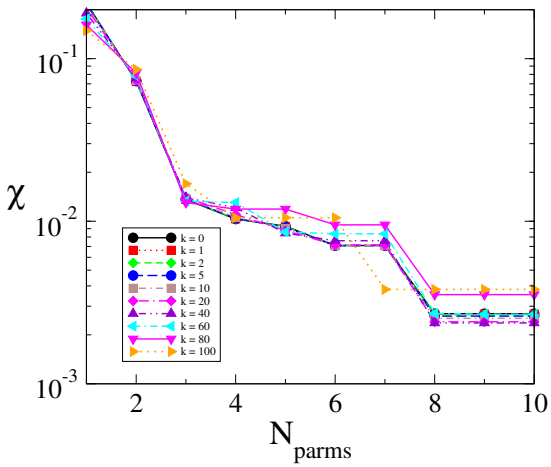

FIG. 6: Average errors χ for the optimal spectral fits as a function of $N_{\rm parms}$ for a sequence of equations of state with second-order phase transitions of various sizes, $0 \leq k \leq 100$.

has a minimum for some v_a. The minimization of $\chi(v_a)$ is carried out numerically in this study using an algorithm based on the Levenberg-Marquardt method [8]. The equation of state, $\epsilon(h, v_a)$ and $p(h, v_a)$, produced by this minimization process is the optimal parametric fit to this equation of state.

Model equations of state created with different numbers of parameters, $N_{\rm parms}$, produce different error minima, $\chi^2(v_a, N_{\rm parms})$. Those with larger $N_{\rm parms}$ generally produce smaller errors, and therefore provide better approximations to the original tabulated equation of state. The minimum values of $\chi(N_{\rm parms})$ for the causal piecewise-analytic representations of the exemplar equations of state with first-order phase transitions are shown as functions of $N_{\rm parms}$ in Fig. 3 for a range of discontinuity sizes, $0 \leq k \leq 100$. Figure 4 shows the analogous results for the exemplar equations of state with second-order phase transitions. The results for the causal spectral representations of the exemplar equations of state with first- or second-order phase transitions are shown in Figs. 5 and 6 respectively.

III. DISCUSSION

The results in Figs. 3 and 4 show that the piecewise-analytic parametric fits to the exemplar equations of state are convergent, in the sense that the average errors $\chi(N_{\rm parms})$ decrease monotonically as the number of parameters $N_{\rm parms}$ increases. These results also show that the accuracies of the piecewise-analytic representations do not depend strongly on the size of the discontinuities. The piecewise-analytic representations therefore provide a robust way to represent equations of state with discon-

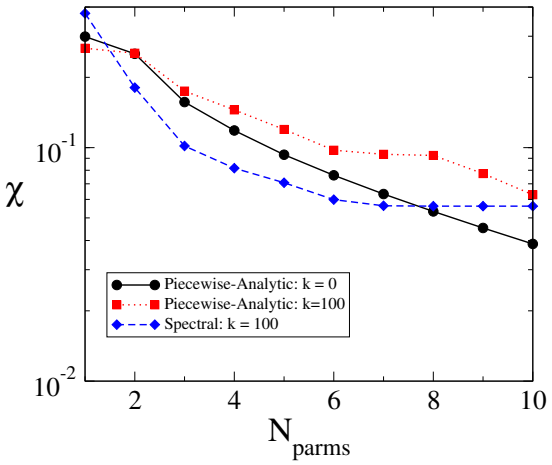

FIG. 7: Comparing modeling errors, $\chi(N_{\rm parms})$, for the optimal causal piecewise-analytic and the causal spectral fits to the exemplar neutron-star equations of state with first-order phase transitions.

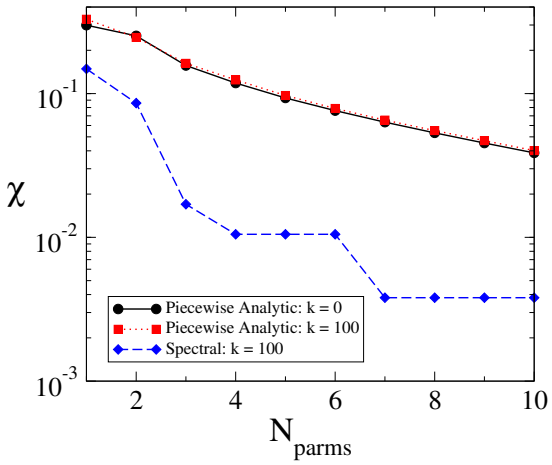

FIG. 8: Comparing modeling errors, $\chi(N_{\rm parms})$, for the optimal causal piecewise-analytic and the causal spectral fits to the exemplar neutron-star equations of state with second-order phase transitions.

tinuities from first- or second-order phase transitions.

The results in Figs. 5 and 6 for the spectral representations are more nuanced. The modeling errors $\chi(N_{\rm parms})$ decrease rapidly as $N_{\rm parms}$ increases to $N_{\rm parms} = 8$ for equations of state with small discontinuities. However for larger values, $N_{\rm parms} > 8$, and for equations of state with larger discontinuities, $\chi(N_{\rm parms})$ becomes more or less constant. These results show that the particular spectral representation used in this study does not provide convergent representations of equations of state with discontinuities caused by phase transitions.

Nevertheless, the modeling errors $\chi(N_{\rm parms})$ for the low-order, $2 \leq N_{\rm parms} \leq 7$, spectral representations are smaller than those of the corresponding piecewise-analytic representations for every exemplar equation of state included in this study. Figures 7 and 8 illustrate the relative accuracies of the two types of parametric representation for the equations of state with first- or second-order phase transitions respectively. While these spectral representations are not convergent, these results show that they are still the mose accurate choice when using low-order parametric fits. The errors in the $N_{\rm parms} = 3$ spectral fits, for example, are fairly small, $0.012 \leq \chi \leq 0.072$, for all the phase transitions studied here. Until the quality and quantity of observational data are improved to allow more accurate determinations of the equation of state, the low-order spectral representations are likely to be the best choice.

It is not clear why the spectral representations fail to converge for equations of states with discontinuities. The basis functions used in the particular spectral representation used here are simple powers of $\log(h/h_0)$, see Eq. (B14). This spectral expansion is therefore similar in form to a Taylor expansion of the velocity function. The radius of convergence of the Taylor expansion of this function would not extend into the high density region beyond the discontinuity caused by a phase transition. It is possible that the spectral expansions using these power-law spectral basis functions fail to converge for a similar reason. If this is the problem, then changing basis functions to Chebyshev polynomials or Fourier basis functions whose domains span the phase transition point would likely improve the convergence properties of the spectral representations.

In cases where a strong first-order phase transition is present, better accuracy and numerical convergence could also be achieved by dividing the equation of state into a low-density domain with pressures and energy densities below the phase transition point, and a second high-density domain with pressures and densities above that point. In the low-density domain, $h_0 \leq h \leq h_T$, the spectral expansion defined in Eqs. (B4)–(B13) could be used. In the high-density domain a separate but similar spectral expansion could be used:

$$p(h) \;=\; p_T + (\bar{\epsilon}_T c^2 + p_T) \int_{h_T}^{h} \bar{\mu}(h')\, dh', \qquad (2)$$

$$\epsilon(h) \;=\; -\frac{p(h)}{c^2} + \left(\bar{\epsilon}_T + \frac{p_T}{c^2}\right) \bar{\mu}(h), \qquad (3)$$

where $p_T = p(h_T)$ and $\bar{\epsilon}_T$ represent the point on the equation of state curve just above the phase transition point. The quantity $\bar{\mu}(h)$ used in these expressions is given by

$$\bar{\mu}(h) = \exp\left\{ \int_{h_T}^{h} \left[2 + \bar{\Upsilon}(h')\right]\, dh' \right\}, \qquad (4)$$

while the velocity function $\bar{\Upsilon}(h)$ used in the high-density domain is given by,

$$\bar{\Upsilon}(h, \upsilon_a) = \exp\left\{ \sum_{a=1}^{\bar{N}_{\rm parms}} \bar{\upsilon}_a \Phi_a(h) \right\}, \qquad (5)$$

for some suitable choice of basis functions $\Phi_a(h)$.

The single domain spectral expansions considered in this study are defined by the values of the $N_{\rm parms}$ spectral parameters υ_a. The two-domain spectral expansions are defined by the values of the original $N_{\rm parms}$ spectral parameters υ_a, plus the $\bar{N}_{\rm parms}$ spectral parameters $\bar{\upsilon}_a$, plus two additional parameters h_T and $\bar{\epsilon}_T$ that determine where the phase transition is located and the size of the energy-density discontinuity at that point. Thus the number of parameters needed to specify the equation of state using this two-domain approach grows from $N_{\rm parms}$ to $N_{\rm parms} + \bar{N}_{\rm parms} + 2$. The cost of going to a two-domain spectral representation could only be justified if sufficient accuracy could not be achieved using a single-domain representation with the same total number of parameters.

Appendix A: Exemplar Equations of State

The exemplar equations of state used in this study were constructed by introducing discontinuities into the relatively smooth GM1L equation of state, which is based on a mean-field representation of the interactions between nucleons [6]. The basic representation of GM1L used here is a table of energy density and pressure points: $\{\epsilon_i, p_i\}$ for $0 \le i \le N_{\rm table}$. The primary goal of this study is to test the accuracy of parametric representations of equations of state with phase transitions in the nuclear-density range. Consequently only the high-density portion of the GM1L equation of state table is used here, beginning at the table entry, $\{\epsilon_0, p_0\}$, where $\epsilon_0 = 5.08587 \times 10^{13}$ g/cm^3 and $p_0 = 1.20788 \times 10^{32}$ erg/cm^3.

This study uses enthalpy-based representations of the equation of state, so the basic pressure-based GM1L table, $\{\epsilon_i, p_i\}$, must be converted to an enthalpy-based table: $\{\epsilon_i, p_i, h_i\}$. The enthalpy of a relativistic fluid is defined by,

$$h(p) = h_0 + \int_{p_0}^{p'} \frac{dp'}{\epsilon(p')c^2 + p'}. \qquad \text{(A1)}$$

In order to evaluate this integral for the tabulated GM1L equation of state, an interpolation formula must be used to determine the values of $\epsilon(p)$ between table entries. The commonly used pseudo-polytropic interpolation,

$$p = p_i \left(\frac{\epsilon}{\epsilon_i}\right)^{\Gamma_i}, \qquad \text{(A2)}$$

is used here to define this equation of state for energy densities, $\epsilon_i \le \epsilon < \epsilon_{i+1}$, in the intervals between table entries. The constants Γ_i in this expression are defined by

$$\Gamma_i = \frac{\log(p_{i+1}/p_i)}{\log(\epsilon_{i+1}/\epsilon_i)}. \qquad \text{(A3)}$$

The low density value of $h_0 = p(h_0)$ used in this study is determined by evaluating the enthalpy integral in the low-density range using one of the standard lower density neutron-star equations of state [9], with the result $h_0 \approx 1.74067 \times 10^{-2}$. At higher densities the enthalpy can be determined by integrating Eq. (A1) between table entries p_i and p_{i+1} using Eq. (A2). These integrals can be done analytically resulting in a recursion relation for the h_{i+1} table entries [10]:

$$h_{i+1} = h_i + \frac{\Gamma_i}{\Gamma_i - 1} \log\left[\frac{\epsilon_i(\epsilon_{i+1}\, c^2 + p_{i+1})}{\epsilon_{i+1}(\epsilon_i\, c^2 + p_i)}\right]. \qquad \text{(A4)}$$

Discontinuities are inserted into GM1L for this study at a point several times nuclear density where the energy density has the value $\epsilon_T = 8 \times 10^{14}$ g/cm^3. The particular equations of state with discontinuities representing first- or second-order phase transitions are described in Secs. A 1 and A 2 respectively. These exemplar equations of state have discontinuities with a range of sizes from zero to the largest physically relevant phase transition of each type.

1. First-Order Phase Transitions

An equation of state $\epsilon = \epsilon(p)$ is said to have a first-order phase transition at $p = p_T$ if $\epsilon(p)$ is discontinuous at that point. Exemplar equations of state with first-order phase transitions are constructed here by modifying the GM1L equation of state at densities above ϵ_T. For this study the transition density ϵ_T is chosen to be several times nuclear density at the point $\epsilon_T = 8 \times 10^{14}$ g/cm^3.

To ensure the tabulated representations of the exemplar equations of state adequately represent the sharp transitions at the phase transition, points are added to the table entries at the points $\epsilon_T^{\pm} = (1 \pm 10^{-6})\,\epsilon_{\rm T}$, just above and below the phase transition. The corresponding pressure points needed to complete the table entries are given by Eq. (A2): $p_{\rm T}^{\pm} = p_i\,(\epsilon_{\rm T}^{\pm}/\epsilon_i)^{\Gamma_i}$, where $\epsilon_i < \epsilon_T^{\pm} < \epsilon_{i+1}$. Once the GM1L equation of state table has been updated with these two additional phase-transition bracketing points, density offsets $\delta\epsilon_T$ are added to all the table entries with densities above ϵ_T. The result is a tabulated model equation of state with a first-order phase transition.

The neutron-star mass-radius curves produced by equations of state with first-order phase transitions show that stars with central densities above ϵ_T are unstable whenever the density discontinuity $\delta\epsilon_T$ exceeds a certain maximum, $\max(\delta\epsilon_T)$ [11]. The masses of these stars achieve a maximum at the point where the central density equals ϵ_T. Stars with larger central densities are subject to a gravitational instability predicted by general relativity theory. The family of stable neutron stars therefore terminates at this point. In some cases there may be an additional higher density family of stable "hyperon"

or perhaps "quark" stars.[1] Neutron stars with central pressures in the unstable region above ϵ_T can never be observed, so equations of state with density offsets above $\max(\delta\epsilon_T)$ will not be considered in this study. The approximate value of this maximum density offset is given by [11],

$$\max(\delta\epsilon_T) = \frac{1}{3}\left(\epsilon_T + 3\,\frac{p_T}{c^2}\right), \tag{A5}$$

where $p_T = p_i\,(\epsilon_T/\epsilon_i)^{\Gamma_i}$, and $\epsilon_i < \epsilon_T < \epsilon_{i+1}$. The maximum density offset, $\max(\delta\epsilon_T)$, is fairly large for the model first-order phase transitions constructed here: $\max(\delta\epsilon_T)/\epsilon_T \approx 0.504634$.[2]

A family of exemplar equations of state with first-order phase transitions have been constructed for this study with density offsets $\delta\epsilon_T$ having sizes in the range $0 \le \delta\epsilon_T \le \max(\delta\epsilon_T)$. The density offsets used in these models are given by,

$$\delta\epsilon_T = \sigma_k\,\max(\delta\epsilon_T), \tag{A6}$$

where the size of the offsets is determined by

$$\sigma_k = \frac{k}{100}, \tag{A7}$$

for $0 \le k \le 100$. The density offset for each exemplar equation of state is added to all the table entries that exceed the transition density ϵ_T. Figure 1 illustrates some of these exemplar equations of state in a neighborhood of the phase transition point. Figure 9 illustrates the mass-radius curves generated from these exemplar equations of state with first-order phase transitions.

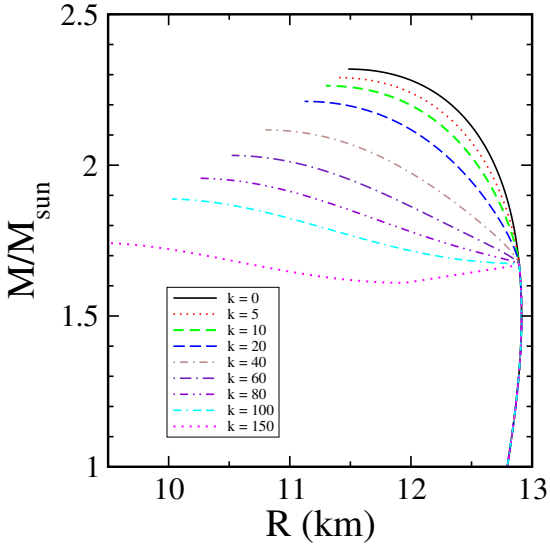

FIG. 9: Examples of mass-radius curves for equations of state with first-order phase transitions. The $k = 0$ curve is based on the unmodified GM1L equation of state, while the $k = 100$ curve corresponds to the equation of state with the maximum density discontinuity defined in Eq. (A5). The $k = 150$ curve illustrates an equation of state with a larger density discontinuity which leads to unstable stars beyond the $\{\epsilon_T, p_T\}$ phase transition point. This $k = 150$ curve also has a disconnected branch of stable relativistic stars at higher densities.

2. Second-Order Phase Transitions

Second-order phase transitions are points on the equation of state curve $\epsilon = \epsilon(p)$ where $\epsilon(p)$ is continuous but $d\epsilon/dp$ is discontinuous. In this study the derivatives of the GM1L equation of state are modified at and above the phase transition density ϵ_T to create a discontinuity that simulates a second-order phase transition. To do this most efficiently, the basic GM1L equation of state table is modified by inserting an additional entry at the point $\{\epsilon_T, p_T\}$. With this addition the second-order phase-transition discontinuity in $d\epsilon/dp$ occurs at one of the tabulated data points.

The derivative of the equation of state, $d\epsilon/dp$, is related to the speed of sound v in a barotropic fluid by $v = (d\epsilon/dp)^{-1/2}$. Any modifications of $d\epsilon/dp$ above the phase transition point must therefore be done in a way that respects causality. A convenient tool for monitoring the causality of sound waves in fluids is the dimensionless velocity function Υ defined by [4]

$$\Upsilon = c^2\,\frac{d\epsilon}{dp} - 1 = \frac{c^2 - v^2}{v^2}. \tag{A8}$$

The propagation of sound waves is causal if and only if $\Upsilon \ge 0$. The velocity function Υ is determined from the basic tabulated GM1L equation of state by evaluating $d\epsilon/dp$ using the interpolation formula in Eq. (A2) at each point in the table. The result is given by

$$\Upsilon_i = \frac{\epsilon_i\,c^2}{p_i\Gamma_i} - 1. \tag{A9}$$

For causal equations of state $\Upsilon \ge 0$, with $\Upsilon = 0$ representing the extreme case of a fluid with sound speed equal to the speed of light, $v^2 = c^2$.

Discontinuities in the slope of the exemplar equations of state were introduced for this study by modifying Υ for densities above the phase transition density, $\epsilon \ge \epsilon_T$, while leaving it unchanged for lower densities. In particular the sound speed was increased by reducing Υ by multiplying it by the factor $1 - \sigma_k$ in this high density region, using the σ_k defined in Eq. (A7). Thus Υ is re-

[1] If the mass-radius curve of these stars has a second inflection point beyond $\{\epsilon_T, p_T\}$ where the mass has a minimum and the radius is decreasing, then stability would be restored and a higher density branch of relativistic stars could exist.

[2] The maximum density offset derived by an analytical analysis in Ref. [11] is 1.5 times the value given in Eq. (A5). Numerical studies, however, show that the effective maximum offset is close to the value given in Eq. (A5).

placed in this high density region by $\tilde{\Upsilon}$ defined by

$$\tilde{\Upsilon} = (1 - \sigma_k)\,\Upsilon. \tag{A10}$$

The maximum physically relevant slope discontinuity at the phase transition point is achieved by setting the sound speed to the speed of light, $v^2 = c^2$ at that point, i.e. by setting $\tilde{\Upsilon} = 0$ there. A family of exemplar equations of state models were constructed for this study that range from the original undistorted GM1L equation of state for $k = 0$, to the extreme equation of state with $\tilde{\Upsilon} = 0$ above the transition density for $k = 100$.

Given $\tilde{\Upsilon}_i$ evaluated at the points of the basic GM1L equation of state table, the modified values of ϵ_i above the phase transition point, $\epsilon_i > \epsilon_T$, can be determined by the recursion relation

$$\epsilon_{i+1} = \epsilon_i \exp\left[(1 + \tilde{\Upsilon}_i)\frac{p_i}{\epsilon_i\, c^2}\log\left(\frac{p_{i+1}}{p_i}\right)\right]. \tag{A11}$$

This expression follows by solving Eq. (A9) for ϵ_{i+1} which contributes to the definition of Γ_i. The pressure points p_i in the equation of state table are not modified. Figure 2 illustrates a few of these exemplar equations of state with larger density-derivative discontinuities in a neighborhood of the second-order phase transition point. Figure 10 illustrates the mass-radius curves generated from these exemplar equations of state with second-order phase transitions.

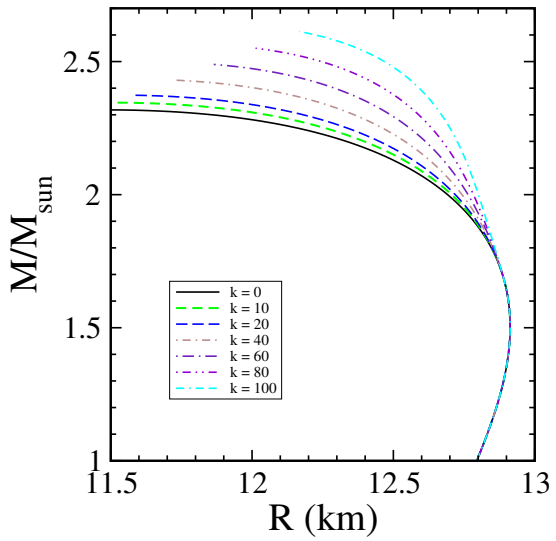

FIG. 10: Examples of mass-radius curves for equations of state with second-order phase transitions. The $k = 0$ curve is based on the unmodified GM1L equation of state, while the $k = 100$ curve is based on the maximal case where the sound speed changes discontinuously to the speed of light above the phase transition.

Appendix B: Causal Parametric Representations

This study uses enthalpy-based representations of the neutron-star equation of state. These representations determine the energy density $\epsilon(h, \upsilon_a)$ and pressure $p(h, \upsilon_a)$ as functions of the enthalpy h and a collection of $N_{\rm parms}$ parameters υ_a for $1 \le a \le N_{\rm parms}$. To be useful tools for representing the physical neutron-star equation of state, these representations must be faithful and they must be causal. Faithful representations have the property that every choice of parameters, υ_a, represents a possible physical equation of state. Conversely every physical equation of state can be represented by some choice, including perhaps an infinite sequence, of parameters [3]. Faithful parametric representations must be convergent as the number of parameters is increased. Causal representations have the property that every choice of parameters generates an equation of state with sound speeds less than or equal to the speed of light [4].

An equation of state has causal sound speeds if and only if the velocity function Υ, defined in Eq. (A8), is non-negative: $\Upsilon \ge 0$. This velocity function can be used as a generating function that determines the full equation of state, so it is a very useful tool for constructing causal parametric representations. The velocity function can be written as a function of the enthalpy:

$$\Upsilon(h) = c^2\frac{d\epsilon}{dp} - 1 = c^2\frac{d\epsilon}{dh}\,\left[\epsilon(h)\,c^2 + p(h)\right]^{-1} - 1. \tag{B1}$$

Given a velocity function, $\Upsilon(h)$, the full equation of state can be reconstructed by solving the following ordinary differential equations for $\epsilon(h)$ and $p(h)$,

$$\frac{dp}{dh} = \epsilon\, c^2 + p. \tag{B2}$$

$$\frac{d\epsilon}{dh} = \left(\epsilon + \frac{p}{c^2}\right)\left[\Upsilon(h) + 1\right], \tag{B3}$$

The first, Eq. (B2), follows from the definition of the enthalpy in Eq. (A1), while the second, Eq. (B3), follows from the definition of $\Upsilon(h)$ in Eq. (B1). These equations can be reduced to quadratures:

$$p(h) = p_0 + (\epsilon_0\, c^2 + p_0)\int_{h_0}^{h}\mu(h')\,dh', \tag{B4}$$

$$\epsilon(h) = -p(h) + \left(\epsilon_0 + \frac{p_0}{c^2}\right)\mu(h), \tag{B5}$$

where $p_0 = p(h_0)$ and $\epsilon_0 = \epsilon(h_0)$ represent a point on the equation of state curve, and $\mu(h)$ is given by

$$\mu(h) = \exp\left\{\int_{h_0}^{h}\left[2 + \Upsilon(h')\right]\,dh'\right\}. \tag{B6}$$

Equations (B4)–(B6) determine a causal enthalpy-based equation of state generated by any non-negative velocity function $\Upsilon(h) \ge 0$.

In this study two different types of parametric representations are used. The first type, piecewise-analytic representations, break the relevant domain of enthalpies into $N_{\rm parms}$ subdomains, and then expresses $\epsilon(h,\upsilon_a)$ and $p(h,\upsilon_a)$ in each subdomain as a particular analytic function determined by the parameters. The particular causal piecewise analytic representations used here are described in Sec. B 1. The second type of parametric representation used in this study is a spectral representation that constructs $\epsilon(h,\upsilon_a)$ and $p(h,\upsilon_a)$ from a generating function determined by a linear combination of spectral basis functions. The particular causal spectral representation used here is described in Sec. B 2.

1. Causal Piecewise-Analytic Representations

The first step in constructing the causal piecewise-analytic enthalpy-based representations used in this study is to divide the enthalpy domain relevant for the high density portion of a neutron-star core, $[h_{\rm min}, h_{\rm max}]$, into $N_{\rm parms}$ subdomains with $h_{\rm min} = h_0 < h_1 < ... < h_{n-1} < h_{N_{\rm parms}} = h_{\rm max}$. The representation used in this study makes the subdomains uniformly spaced in $\log h$: $\log(h_{a+1}/h_a) = N_{\rm parms}^{-1} \log(h_{\rm min}/h_{\rm max})$ for all $1 \le a \le N_{\rm parms}$.

The second step is to choose analytical functions $\Upsilon(h,\upsilon_a)$ to approximate $\Upsilon(h)$ in each subdomain. The challenge is to find analytical functions that are reasonably good approximations in each subdomain, and that are simple enough to allow Eqs. (B4) and (B5) to be solved analytically for $\epsilon(h,\upsilon_a)$ and $p(h,\upsilon_a)$. Graphs in Ref. [4] show that $\log\Upsilon$ is more or less proportional to $\log h$ for a collection of model neutron-star equations of state. This fact, together with the need to have simple functions that can be integrated analytically, lead to the following choice for $\Upsilon(h,\upsilon_a)$ [4],

$$\Upsilon(h,\upsilon_a) = \frac{\upsilon_a + 2(h_a - h)}{h}, \tag{B7}$$

in the subdomain $h_{a-1} \le h < h_a$. These velocity functions are non-negative within each subdomain so long as the adjustable parameters are chosen to be non-negative, $\upsilon_a \ge 0$.

The piecewise-analytic representation of the equation of state, $\epsilon(h,\upsilon_a)$ and $p(h,\upsilon_a)$, that corresponds to the $\Upsilon(h,\upsilon_a)$ given in Eq. (B7) is determined by evaluating the integrals in Eqs. (B4)–(B6). Inserting the expression for $\Upsilon(h,\upsilon_a)$ from Eq. (B7) into these integrals gives the following expressions for the equation of state,

$$p(h,\upsilon_a) = p_a + \frac{\left(\epsilon_a\, c^2 + p_a\right) h_a}{\lambda_a + 1}\left[\left(\frac{h}{h_a}\right)^{\lambda_a+1} - 1\right], \tag{B8}$$

$$\epsilon(h,\upsilon_a) = -p(h,\upsilon_a)c^{-2} + \left(\epsilon_a + p_a c^{-2}\right)\left(\frac{h}{h_a}\right)^{\lambda_a}, \tag{B9}$$

in the subdomain $h_a \le h < h_{a+1}$, where

$$\lambda_a = \upsilon_{a+1} + 2h_{a+1}. \tag{B10}$$

The constants $p_a = p(h_a,\upsilon_a)$ and $\epsilon_a = \epsilon(h_a,\upsilon_a)$ are determined from the recursion relations,

$$p_{a+1} = p_a + \frac{\left(\epsilon_a\, c^2 + p_a\right) h_a}{\lambda_a + 1}\left[\left(\frac{h_{a+1}}{h_a}\right)^{\lambda_a+1} - 1\right], \tag{B11}$$

$$\epsilon_{a+1} = -p_{a+1}c^{-2} + \left(\epsilon_a + p_a c^{-2}\right)\left(\frac{h_{a+1}}{h_a}\right)^{\lambda_a}. \tag{B12}$$

The constants $p_0 = p(h_0) \ge 0$ and $\epsilon_0 = \epsilon(h_0) \ge 0$ are determined from the low-density equation of state at the matching point $h = h_0$..

2. Causal Spectral Representations

Spectral methods are very efficient ways to represent smooth functions, providing good accuracy with only a small number of spectral basis functions. This study is designed to test how well spectral representations are able to represent non-smooth functions, i.e. equations of state with phase transitions. Causal spectral representations are generated by a spectral expansions of the velocity function $\Upsilon(h)$:

$$\Upsilon(h) = \exp\left\{\sum_{a=1}^{N_{\rm parms}} \upsilon_a \Phi_a(h)\right\}, \tag{B13}$$

where $\Phi_a(h)$ are a suitable set of spectral basis functions and the constants υ_a are the spectral coefficients. Inserting this expression for $\Upsilon(h)$ into Eqs. (B4)–(B6) produces a causal equation of state determined by the parameters υ_a. Any equation of state constructed in this way automatically produces a velocity function $\Upsilon(h)$ that satisfies the causality condition $\Upsilon(h) \ge 0$.

This study uses the very simple choice of spectral basis functions $\Phi_a(h) = [\log(h/h_0)]^a$, which creates a collection of velocity functions, $\Upsilon(h,\upsilon_a)$, parameterized by υ_a [5]:

$$\Upsilon(h,\upsilon_a) = \Upsilon_0 \exp\left\{\sum_{a=1}^{N_{\rm parms}} \upsilon_a \left[\log\left(\frac{h}{h_0}\right)\right]^a\right\}. \tag{B14}$$

The constant $\Upsilon_0 = \Upsilon(h_0)$ in this expression is evaluated from the low-density portion of the equation of state at the point h_0 using Eq. (A9). Every choice of spectral parameters υ_a in Eq. (B14) determines a non-negative velocity function, and using Eqs. (B4) and (B5) this generating function determines a parameterized enthalpy-based causal equation of state, $\epsilon = \epsilon(h,\upsilon_a)$ and $p = p(h,\upsilon_a)$. These integrals can not be done analytically, however, the integrands are smooth and they can

be evaluated numerically very accurately and efficiently using Gaussian quadrature. If the spectral expansion in Eq. (B13) is convergent, then every causal equation of state can be represented in this way by including enough terms in the spectral expansion, i.e. by choosing $N_{\rm parms}$ sufficiently large. However as this study shows, the spectral representations of equations of state with large phase transitions are not convergent for representations based on the particular spectral expansion in Eq. (B14).

Acknowledgments

I thank Jimmy Zhou for helping me debug parts of the code used in this study, and Steve Lewis for numerous conversations related to this study, and for helpful comments and suggestions on an earlier draft of this paper. This research was supported in part by the National Science Foundation grant 2012857 to the University of California at San Diego.

[1] L. Lindblom, Astrophys. J. **398**, 569 (1992).
[2] J. S. Read, B. D. Lackey, B. J. Owen, and J. L. Friedman, Phys. Rev. **D79**, 124032 (2009).
[3] L. Lindblom, Phys. Rev. D **82**, 103011 (2010).
[4] L. Lindblom, Phys. Rev. D **97**, 123019 (2018).
[5] L. Lindblom, Phys. Rev. D **105**, 063031 (2022).
[6] S. Typel, G. Ropke, T. Klahn, D. Blaschke, and H. H. Wolter, Physical Review C **81**, 015803 (2010).
[7] J. R. Oppenheimer and G. M. Volkoff, Phys. Rev. **55**, 374 (1939).
[8] W. H. Press, S. A. Teukolsky, W. T. Vetterling, and B. P. Flannery, *Numerical Recipes in FORTRAN* (Cambridge University Press, Cambridge, England, 1992), 2nd ed.
[9] G. Baym, C. Pethick, and P. Sutherland, Astrophys. J. **170**, 299 (1971).
[10] L. Lindblom and N. M. Indik, Phys. Rev. D **86**, 084003 (2012).
[11] L. Lindblom, Phys. Rev. D **58**, 024008 (1998).